ACS Macro Letters

pubs.acs.org/macroletters Letter

Margination of 2D Platelet Microparticles in Blood

Jordan Thomas Lovegrove, Radhika Raveendran, Patrick Spicer, Stephan Förster, Christopher J. Garvey, and Martina H. Stenzel*

Cite This: ACS Macro Lett. 2023, 12, 344−349 Read Online

ACCESS | Metrics & More | Article Recommendations | Supporting Information

ABSTRACT: Margination describes the movement of particles toward the endothelial wall within blood vessels. While there have been several studies tracking the margination of spherical particles in blood, the behavior of anisotropic particle shapes is not well described. In this study 2D platelet particles which possess many attractive qualities for use as a drug delivery system, with their high surface area allowing for increased surface binding activity, were directly monitored and margination quantified. The margination propensity of 1 and 2 μm 2D platelet particles was contrasted to that of 2 μm spherical particles at apparent wall shear rates (WSRs) of 50, 100, and 200 s^{-1} by both directly tracking labeled particles using fluorescent microscopy as well as using small-angle X-ray scattering (SAXS). For fluorescence studies, margination was quantified using the margination parameter *M*, which describes the number of particles found closest to the walls of a microfluidic device, with an *M*-value of 0.2 indicating no margination. Increased margination was seen in 2D platelet particles when compared to spherical particles tested at all flow rates, with *M*-values of 0.39 and 0.31 seen for 1 and 2 μm 2D platelet particles, respectively, while 2 μm spherical particles had an *M*-value of 0.21. Similarly, margination was observed qualitatively using SAXS, with increased scattering seen for platelet particles near the microfluidic channel wall. For all particles, increased margination was seen at increasing shear rates.

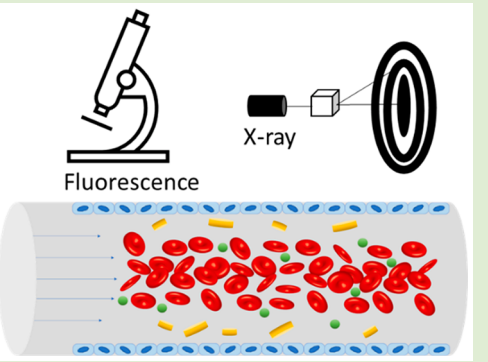

Margination is a phenomenon characterized by the movement of particles or cells in blood toward the wall of the vessel. This occurs primarily in the microvasculature, where blood does not behave like a Newtonian fluid. In blood vessels with diameters less than 500 μm, red blood cells (RBCs) move toward the center of the vessel due to wall-induced hydrodynamic lift.[1−3] The migration of RBCs into the center of the channel results in the formation of a viscous phase consisting of RBCs and a less viscous phase close the vessel walls containing very few RBCs—known as the cell-free layer (CFL). Margination has been well documented for white blood cells and platelets within the body, mediating key steps in blood clotting and in the immune response.[2,4] Particle margination is determined by blood-related factors such as vessel diameter, wall shear rate (WSR), blood hematocrit, and intrinsic particle properties such as size, shape, density, and stiffness.[5−11] Designing particles that can effectively marginate and reside close to the vessel walls has many potential applications in drug delivery.[1,3,9] Particles able to interact with the vascular wall allow a greater chance for these particles to leave the vessel and travel to the desired site. This is especially relevant for the microvascular architecture surrounding tumors, which have leaky vessels with large fenestrations up to 200 nm.[12−15]

Blood hematocrit (volume percentage of red cells in blood) and WSR (change in velocity at the various layers of blood fluid) vary in the body according to vessel type and size. Hematocrit typically ranges from 30 to 45% systematically; however, in the microvasculature, blood hematocrit can drop below 20% of the supply vessels, with a 30 μm vessel typically having 16−20% hematocrit.[2,12,16−18] Likewise, WSR varies in the microvasculature with ranges from 100 to 1600 s^{-1} in arterioles—dependent on measurement site and size of the vessel—but is at its highest in capillaries and arterioles.[19−21]

Similarly, intrinsic properties of the particle also influence margination, namely, size, shape, and density. Several studies indicate that particles between 500 nm and 5 μm are needed for optimal margination to occur; however, margination has been described for small, dense, gold nanoparticles as well.[1,3,5,6,8,9,16,18,22,23] While some theoretical studies indicate that nonspherical particles with high aspect ratios marginate more than spheres of equivalent size, the effect of particle stiffness has not been thoroughly explored, but simulations of stiff particles and malaria-effected cells indicate that stiffer particles lead to more margination.[8,24]

Despite several theoretical and experimental studies attempting to draw correlations between these factors and

Received: December 11, 2022
Accepted: February 16, 2023
Published: February 23, 2023

margination, the disparity in experimental conditions and assumptions made makes trends hard to distinguish. The effect of flow rate on margination is not clear, with several studies describing both an increase in margination with flow velocity and the opposite.[10,16] This is due to highly divergent experimental techniques used, such as several surface adhesion studies attempting to describe margination and relatively little direct tracking of particles under flow conditions.[3,9,11,23,25−30] In these publications, fluorescent microscopy was used to monitor the position of the particles in the blood flow. In this letter, we track platelet nanoparticles directly using fluorescent microscopy as well as SAXS, which has not yet been employed. While the margination of nonspherical particles toward the blood vessel has been observed earlier, we use here platelets, a term for polymeric 2D microparticles obtained by crystallization-driven self-assembly.[31,32] These polymer platelets are versatile as the size can be controlled by living growth, while it is possible to load these structures with drugs.[33,34]

Therefore, a biocompatible crystalline polymer poly(L-lactic acid) (PLLA) was synthesized using ring-opening polymerization (ROP) which was then chain extended using single electron transfer transfer-living radical polymerization (SET-LRP), with a statistical block copolymer consisting of poly(dimethyl acrylamide) (PDMA) and poly(*tert*-butyoxycarbonyl amino ethyl acrylate) (PTAEA). The *tert*-butyl-protecting group was then deprotected using trifluoroacetic acid to reveal a functional amine group (aminoethyl acrylate, PAEA) and the final polymer $PLLA_{36}$-*b*-P(DMA_{202}-*co*-AEA_{25}) (Figure 1, SI, Figures S1−S4 and Schemes S1−S3). This

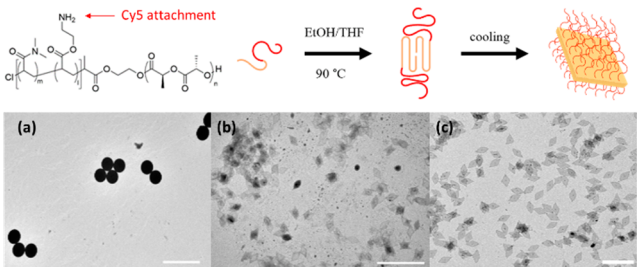

Figure 1. Preparation of platelets in ethanol (EtOH) and tetrahydrofuran (THF) and their analysis via TEM. TEM micrographs of (a) latex microsphere, (b)$L_{n,major}$ = 1.3 μm assembled platelet (1 μm), and (c) $L_{n,major}$ = 2.3 μm assembled platelet (2 μm). Scale bar = 5 μm. More images can be seen in the Supporting Information.

polymer was then assembled into 2D platelet particles using a crystallization-driven self-assembly method modified from the literature. Different EtOH and THF solvent mixtures were used to obtain platelets of different sizes as outlined in the Supporting Information (Figure 1 and SI Figures S5−S6 and Table S1).[35,36] The thickness of the crystalline core is around 17−20 nm. The major length of these diamond-shaped platelets is 1.3 or 2.3 μm, while the minor length is 0.8 and 1.3 μm, respectively, making these materials flexible (SI, Table S1).

After assembly, the platelets were then conjugated with Cy5-COOH fluorescent dye in water (SI, Scheme S4 and Figure S7). As a control to determine the margination ability of platelet particles, 2 μm of polystyrene (PS) latex spheres was purchased, which are commonly used in control experiments as they are not supposed to display any margination.[30] The latex spheres were adjusted to a concentration of 10 mg mL^{-1} and then fluorescently modified by encapsulating Nile Red dye within the hydrophobic core of the solid particle. TEM was used to confirm the sizes and morphologies of the 2D platelet particles synthesized. These platelets were transferred into water by centrifugation and resuspension in water (Figure 1).[37] The different particles will have different fluorescence intensities and different emission maxima (Cy 5 vs Nile Red), and absolute values are moreover difficult to determine. However, here only the fluorescence distribution within one sample is compared, and it is not necessary to adjust the fluorescence between all three solutions.

In this study we used horse blood as it is readily available and sufficiently similar to human blood.[38] Whole horse blood purchased from Edwards was washed with PBS solution to remove unwanted proteins and other blood components and adjusted to a 15% hematocrit solution which was then resuspended in Optiprep (density gradient medium), phosphate buffer (PBS), and glucose medium to simulate the density of blood. Confirmation that the CFL could be formed was verified using light microscopy, with an absence of RBCs seen close to the channel wall to ensure its presence at biologically relevant shear rates as seen in the SI (Figure S8).

Fluorescently labeled platelet particles at a concentration of 10 mg/mL were then mixed with 15% hematocrit blood and flowed through the rectangular microfluidic device (100 μm wide and 160 μm in height) at shear rates of 50, 100, and 200 s^{-1}. The microfluidic channel was divided into 10 equal segments of 10 μm, and the number of particles seen in each 10 μm segment was counted and the *y*-position normalized and graphed as seen in Figure 2 (SI, Figure S9).

Particle frequency was found to be significantly higher in the 10 μm segments closest to the walls of the microfluidic devices

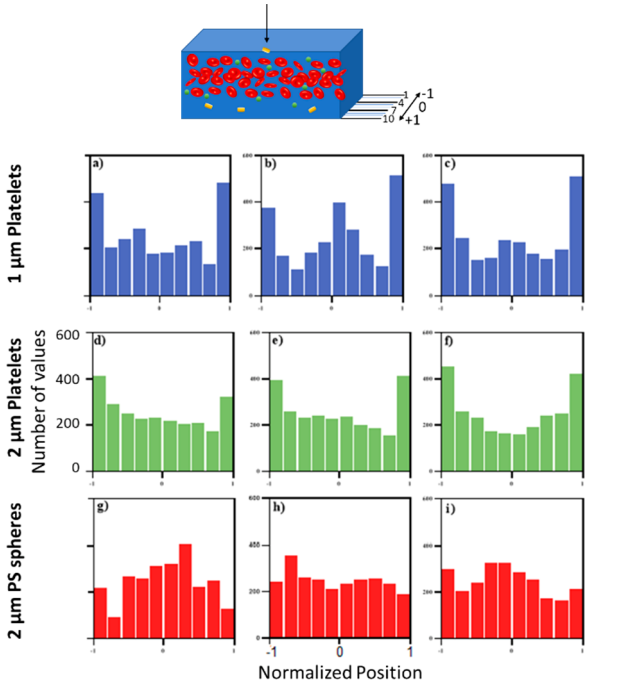

Figure 2. Particle margination under flow in microfluidic devices determined by particle count per segment normalized to the *y*-position for 1 μm platelets (a, b, c), 2 μm platelets (d, e, f), and 2 μm spheres (g, h, i) at shear rates of 50 s^{-1}, 100 s^{-1}, and 200 s^{-1} in 15% hematocrit horse blood. At least 3000 particles were counted for each particle shape and shear rate.

https://doi.org/10.1021/acsmacrolett.2c00718
ACS Macro Lett. 2023, 12, 344−349

for both the 1 and 2 μm platelets, but this trend was not seen for the 2 μm PS latex spheres. To quantify the margination propensity of the microparticles, the margination parameter as described by Carboni et al. was used, where

$$M = \frac{P_{1^{st}\ \text{segment}} + P_{10^{th}\ \text{segment}}}{\sum_{i^{th}\ \text{segment} \in [1,10]} P_i}$$

where P is the particle count in each segment.[30,37] The number of particles across all 10 segments ($\sum_{i^{th}\ \text{segment} \in [1,10]} P_i$) is then compared to the number of particles in the 1st and the 10th segment and thus the closest to the wall. Even distribution would result in a margination parameter (M) value of 0.2; therefore, values greater than 0.2 indicate there are more particles found closer to the walls of the channel. This parameter M serves as a simple tool to compare the margination propensity of different particle shapes and sizes under different conditions such as channel size and flow rate. Particles were measured approximately 10 mm from the outlet position to ensure that the stream was fully formed. For each experimental condition, 3000 particles were measured, and their position was normalized as seen in Figure 2. The average and standard deviation of the margination parameter, M, was calculated based on every 1000 particles tracked, as seen in Figure 3.

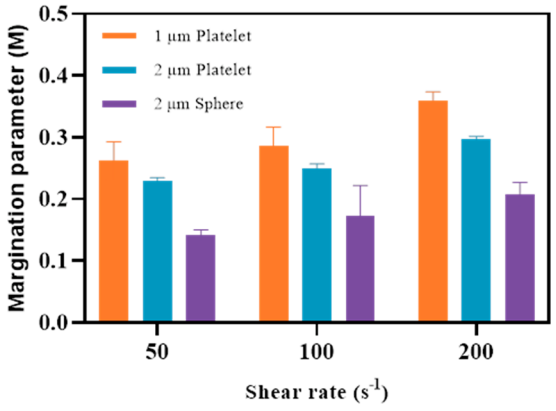

Figure 3. Comparison of margination parameter M between 1 μm platelets, 2 μm platelets, and 2 μm latex spheres at apparent shear rates of 50 s^{-1}, 100 s^{-1}, and 200 s^{-1}.

Interestingly, the margination propensity of platelets was far higher than spherical particles at all flow rates, and 1 μm platelets were seen to marginate more with increasing shear rate, increasing from M = 0.34 at 50 s^{-1} to M = 0.39 at 200 s^{-1}. This was also seen for 2 μm platelets, where margination increased with an increase in shear rate, and a range of M between 0.29 and 0.34, slightly less than seen in 1 μm platelets. However, for 2 μm spheres, low M values ranging from 0.14 to 0.21 were seen, indicating no margination and that platelet particles marginate much more than spheres of equivalent sizes at all shear rates. When compared to experiments conducted by Carboni et al., 2.11 μm spherical PS particles were found to marginate more than 0.53 and 0.87 μm spherical particles. The M values for the large spheres were measured to be 0.28 in a solution of 35% hematocrit, higher than the amount used here.[30] Slight increases in the margination parameter can be seen for all particles as shear rate increases, in agreement with the literature.[8,39] Interestingly, clear increases in margination were not seen for platelets with increasing size, contrary to the trend commonly reported in both experimental and simulation studies. These studies suggest that particle margination increases with size, with the best margination attributes seen from microparticles, specifically oblate and rod-shaped particles.[40,41] However, the increased margination of the smaller 1 μm particles over the larger 2 μm particles has not been reported and could be due to a number of factors such as buoyancy or another shape-related factor. The significant margination of platelet particles, when compared to the PS latex spheres, is likely due to the particle shape and stiffness, with the high surface area to volume and pseudo 2D shape. This relatively high rigidity compared to noncrystalline particles and high surface area leads to more torque experienced by the platelets, resulting in more tumbling to the CFL due to inelastic collisions with RBCs. While higher shear rates lead to more margination, a longer distance is needed for the flow to completely develop. In work conducted by Carboni et al., a distance of 10 mm from the inlet position was found to show more particle margination compared to positions near the inlet and 2 mm from the inlet, and this is consistent with vessel branching inside the body, which occurs approximately every 10 mm.[30,42] If the flow is not fully developed, Brownian motion can limit the inhomogeneity of the final margination profile. The Brownian effects were found to be nonconsequential in this system, as the Peclet number calculated by

$$P_e = \frac{6\pi\eta_0\dot{\gamma}a^3}{kT}$$

which is the ratio of Brownian-driven versus shear-driven time scales, where η_0 is the viscosity of the solution, $\dot{\gamma}$ the shear rate, a the particle radius, k the Boltzmann constant, and T the temperature. For values of P_e < 100, Brownian motion is significant and will influence the margination of particles in flow. At P_e > 100, the effects of Brownian motion become less prominent. For all shear rates measured, P_e > 100 (SI, Table S2), indicating particle diffusion was not a significant contributor to particle margination.[43]

In this work, we wanted to complement margination seen in the fluorescent microscopy with small-angle X-ray scattering (SAXS). While SAXS is widely applied to observe the alignment of nonspherical nanoparticles in flow, it has not yet been used for similar purposes in blood.[44,45] SAXS allows the whole dispersion volume of the channel to be measured. This means in contrast to microscopy experiments there is no need to choose a focal point within the channel or exclude out of focus particles, eliminating the source of potential tracking biases that can arise. Consequently, the volume of particles measured using SAXS for each point is a much larger (20 × 200 μm) area due to the limits of X-ray microfocus, whereas microscopy experiments included ten 10 μm segments. X-ray compatible microfluidic devices were fabricated using a method outlined by Evans et al., with the same channel dimensions as those used in fluorescence microscopy experiments.[42] Due to the high X-ray scattering of horse blood and the low electron density of PLLA-based particles, modification of the platelet particles was needed to increase the electron density and resulting scattering intensity. Platelets were first reacted with poly(2-hydroxyethyl acrylate) (PHEA) using EDC/NHS coupling outlined in the SI, Schemes S5 and S6. The RAFT agent present on the PHEA was then used as an attachment point for the gold nanoparticles (GNPs) through

https://doi.org/10.1021/acsmacrolett.2c00718
ACS Macro Lett. 2023, 12, 344−349

strong gold−thiol bonding (Figure 4).[46] GNP attachment was confirmed by imaging using TEM showing around 500−600

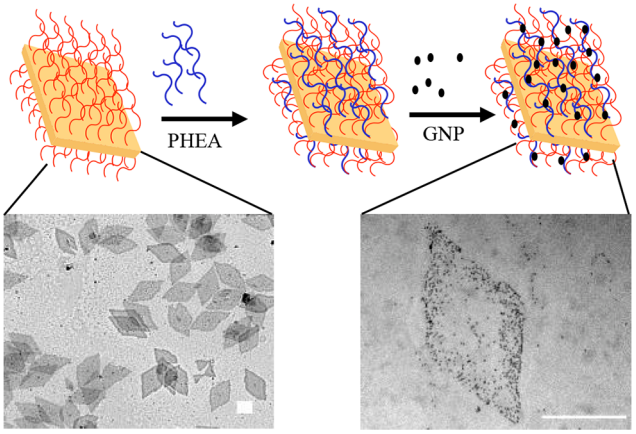

Figure 4. Modification scheme of (a) $PLLA_{36}$-*b*-($PDMA_{202}$-*co*-$PAEA_{25}$) with PHEA and GNP to increase SAXS contrast and (b) TEM micrograph of GNP-coated platelets. Scale bar = 1 μm.

GNP per platelet per larger platelet. Unreacted GNP has been removed by centrifugation, yet some free GNP will not influence the analysis. Similar to fluorescence, the absolute number among the three systems is not crucial, as margination will only be measured within a sample system. Additionally, the attachment of these GNPs also acts to increase the density of the particles, which will also impact particle margination. It is suggested that denser nanoparticles will marginate less, which means that any margination observed here should be even more noticeable in GNP-free platelets.[28] Gold nanoparticles were not attached onto the latex spheres, as the scattering of the spheres was sufficient enough to be seen in blood.

A modified microfluidic device was fabricated to be compatible with SAXS measurements following the protocols described by Evans et al.[47] Kapton tape was introduced into the PDMS microfluidic device, to create a small window where the X-ray scattering used would not pass through any PDMS (Figure 5j). SAXS measurements were conducted under the same conditions as the fluorescent microscopy experiments, with the X-ray source aligned 90° from the direction of flow.

Four points along the *y*-axis of the channel were chosen by scanning at six different sites along the channel outlined in Figure 5 to find the edges and ensure all points that were to be measured were within the channel. Backgrounds were taken of horse RBCs with 15% hematocrit in Optiprep at the same coordinates of measurement at each flow rate measured. Higher transmission can be seen closest to the channel edges for the GNP-coated platelet particles, with the opposite seen for PS latex spheres. The signal of strength at the four positions chosen after background subtraction were then compared to determine the areas of the channel with the highest concentration of particles, as an indicator of margination. These results were then used to confirm results seen using fluorescence microscopy. It is evident that there is a difference in positions 1 and 4, which is the result of some gravitational effects and the difficulty of positioning the X-ray beam.

Particle scattering can be seen to be the highest at points closest to the channel edge (positions 1 and 4) for both 1 and 2 μm platelets at all flow rates, when compared to positions taken in the center of the channel as seen in Figure 5j. However, this same trend is not seen with the 2 μm spheres

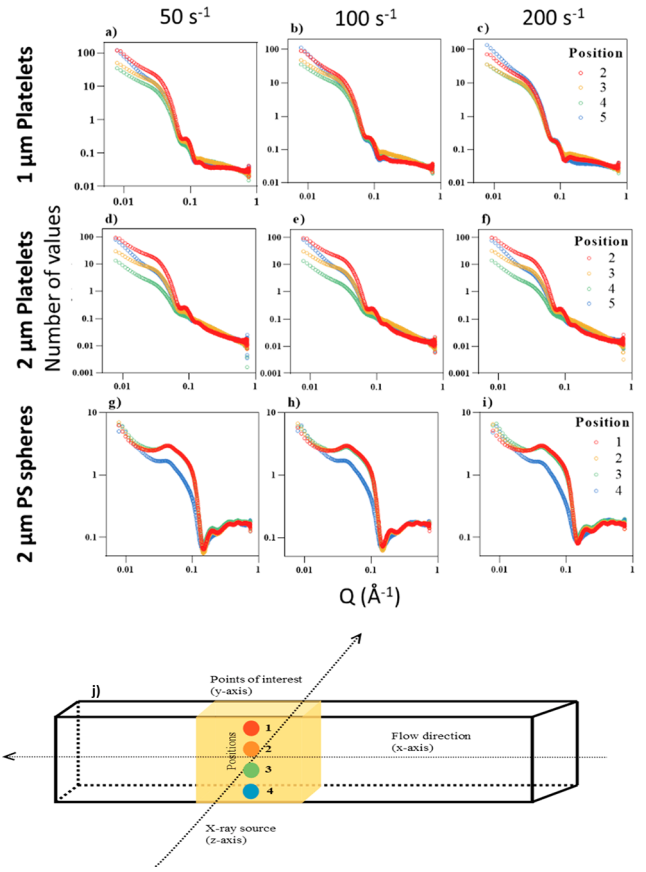

Figure 5. SAXS curves at each position in a microfluidic device for 1 μm platelets (a, b, c), 2 μm platelets (d, e, f), and 2 μm spheres (g, h, i) at shear rates of 50 s^{-1}, 100 s^{-1}, and 200 s^{-1} in blood. (j) Schematic of margination tracking using SAXS setup and data collection points.

(positions 1 and 4), with obvious signal increases at the positions closest to the channel edge only seen in the fastest shear rate measured. Much less scattering intensity was seen in the 2 μm spheres when compared to the GNP-coated platelets due to the low electron density of the PS latex spheres. Intensity at positions close to the wall were 2−10 times larger than positions close to the core of the stream for all flow rates in both 1 and 2 μm platelets. These results match those seen in fluorescent microscopy, with margination seen in platelet samples and very little seen in the spherical particles. This shows there is a strong preference for platelet particles to reside close to the channel wall. Distinctive GNP scattering can be seen at high *Q* ranges for platelets coated with GNPs, helping with X-ray contrast; however, this trend of higher scattering at edge positions is not seen when GNPs flowed through blood by themselves as a control (SI, Figure S10). As a control, the 17 nm diameter GNPs alone were found to flow in the center of the stream preferentially, which algins with previously described systems describing the flow of gold nanoparticles.[28] Little variance in intensity is seen as a function of the *y* axis position. These results confirm that the enhanced margination observed in the GNP-functionalized platelets is due to platelet margination, not an artifact of GNP conjugation. However, while SAXS can provide qualitative confirmation of margination, quantification is not possible and is therefore most useful for observing margination in systems where microscopy is not feasible.

https://doi.org/10.1021/acsmacrolett.2c00718
ACS Macro Lett. 2023, 12, 344−349

The margination of 1 and 2 μm platelet particles and 2 μm spheres in blood was monitored using fluorescence microscopy and SAXS analysis. Higher margination was seen with increasing shear rate with both techniques. Both 1 and 2 μm platelet particles were found to marginate much more than 2 μm PS latex spheres at all shear rates measured due to their shape and resulting flow dynamics that result in more nonelastic collision events between particles and RBCs. Interestingly, the highest margination rates were seen in 1 μm platelets at all shear rates measured, in contrast to trends that indicate larger particles marginate more than smaller particles. It should be noted here that margination is also a function of the hematocrit value, and more margination is expected at higher values. The value chosen here is relatively low to enable SAXS analysis, as higher amounts of RBC might hamper analysis. These findings show that platelet particles marginate far more than spherical particles of comparable size in blood under physiological conditions and have the potential for increased circulation time in the body and preferential accumulation of particles at tumors.

■ ASSOCIATED CONTENT

Supporting Information

The Supporting Information is available free of charge at https://pubs.acs.org/doi/10.1021/acsmacrolett.2c00718.

Synthesis of the SET-LRP initiator, polymer synthesis, NMR, SEC, crystallization-driven self-assembly, microfluidic device fabrication, fluorescent microscopy, particle tracking, SAXS (PDF)

■ AUTHOR INFORMATION

Corresponding Author

Martina H. Stenzel − *Centre for Advanced Macromolecular Design, School of Chemistry, The University of New South Wales, Sydney, NSW 2052, Australia;* orcid.org/0000-0002-6433-4419; Email: m.stenzel@unsw.edu.au

Authors

Jordan Thomas Lovegrove − *Centre for Advanced Macromolecular Design, School of Chemistry, The University of New South Wales, Sydney, NSW 2052, Australia;* orcid.org/0000-0002-8971-4821

Radhika Raveendran − *Centre for Advanced Macromolecular Design, School of Chemistry, The University of New South Wales, Sydney, NSW 2052, Australia*

Patrick Spicer − *School of Chemical Engineering, The University of New South Wales, Sydney, NSW 2052, Australia;* orcid.org/0000-0002-8562-3906

Stephan Förster − *Forschungszentrum Jülich GmbH, 52428 Jülich, Germany;* orcid.org/0000-0002-7323-2449

Christopher J. Garvey − *Australian Centre for Neutron Scattering, Australia Nuclear Science and Technology Organization, Lucas Heights, NSW 2234, Australia; Technische Universität München, Forschungsneutronenquelle Heinz Maier-Leibnitz FRM II and Physik Department E13, 85747 Garching, Germany;* orcid.org/0000-0001-6496-7008

Complete contact information is available at: https://pubs.acs.org/10.1021/acsmacrolett.2c00718

Author Contributions

CRediT: **Jordan Lovegrove** data curation (lead), formal analysis (lead), investigation (lead), methodology (lead), writing-original draft (lead); **Radhika Raveendran** investigation (supporting), methodology (supporting), visualization (supporting); **Patrick T. Spicer** formal analysis (supporting), methodology (supporting), writing-review & editing (supporting); **Stephan Förster** conceptualization (supporting), supervision (supporting), validation (supporting), writing-review & editing (supporting); **Christopher J. Garvey** formal analysis (supporting), funding acquisition (supporting), methodology (supporting), project administration (supporting), supervision (supporting), writing-review & editing (supporting); **Martina H. Stenzel** conceptualization (lead), funding acquisition (lead), project administration (lead), supervision (lead), writing-review & editing (lead).

Notes

The authors declare no competing financial interest.

■ ACKNOWLEDGMENTS

The authors would like to thank the staff of the Electron Microscopy Unit (EMU) of the Mark Wainwright Analytical Centre. We acknowledge the support of the Australian Research Council (ARC DP190102528, FL200100124). This research was undertaken on the SAXS beamline at the Australian Synchrotron, part of ANSTO.

■ REFERENCES

(1) Gomez-Garcia, M. J.; Doiron, A. L.; Steele, R. R. M.; Labouta, H. I.; Vafadar, B.; Shepherd, R. D.; Gates, I. D.; Cramb, D. T.; Childs, S. J.; Rinker, K. D. Nanoparticle Localization in Blood Vessels: Dependence on Fluid Shear Stress, Flow Disturbances, and Flow-Induced Changes in Endothelial Physiology. *Nanoscale* **2018**, *10* (32), 15249−15261.

(2) Pries, A. R.; Fritzsche, A.; Ley, K.; Gaehtgens, P. Redistribution of Red Blood Cell Flow in Microcirculatory Networks by Hemodilution. *Circ. Res.* **1992**, *70* (6), 1113−1121.

(3) Carboni, E.; Tschudi, K.; Nam, J.; Lu, X.; Ma, A. W. K. Particle Margination and Its Implications on Intravenous Anticancer Drug Delivery. *AAPS PharmSciTech* **2014**, *15* (3), 762−771.

(4) Chachanidze, R. Collective Phenomena in Blood Suspensions. *Doctoral Thesis*; 2018.

(5) Thompson, A. J.; Mastria, E. M.; Eniola-Adefeso, O. The Margination Propensity of Ellipsoidal Micro/Nanoparticles to the Endothelium in Human Blood Flow. *Biomaterials* **2013**, *34* (23), 5863−5871.

(6) Gentile, F.; Chiappini, C.; Fine, D.; Bhavane, R. C.; Peluccio, M. S.; Cheng, M. M. C.; Liu, X.; Ferrari, M.; Decuzzi, P. The Effect of Shape on the Margination Dynamics of Non-Neutrally Buoyant Particles in Two-Dimensional Shear Flows. *J. Biomech* **2008**, *41* (10), 2312−2318.

(7) Hou, H. W.; Bhagat, A. A. S.; Lin Chong, A. G.; Mao, P.; Wei Tan, K. S.; Han, J.; Lim, C. T. Deformability Based Cell Margination - A Simple Microfluidic Design for Malaria-Infected Erythrocyte Separation. *Lab Chip* **2010**, *10* (19), 2605−2613.

(8) Chang, H. Y.; Yazdani, A.; Li, X.; Douglas, K. A. A.; Mantzoros, C. S.; Karniadakis, G. E. Quantifying Platelet Margination in Diabetic Blood Flow. *Biophys. J.* **2018**, *115* (7), 1371−1382.

(9) Carboni, E. J.; Bognet, B. H.; Cowles, D. B.; Ma, A. W. K. The Margination of Particles in Areas of Constricted Blood Flow. *Biophys. J.* **2018**, *114* (9), 2221−2230.

(10) Namdee, K.; Thompson, A. J.; Charoenphol, P.; Eniola-Adefeso, O. Margination Propensity of Vascular-Targeted Spheres from Blood Flow in a Microfluidic Model of Human Microvessels. *Langmuir* **2013**, *29* (8), 2530−2535.

(11) Ta, H. T.; Truong, N. P.; Whittaker, A. K.; Davis, T. P.; Peter, K. The Effects of Particle Size, Shape, Density and Flow Characteristics on Particle Margination to Vascular Walls in Cardiovascular Diseases. *Expert Opin Drug Deliv* **2018**, *15* (1), 33−45.
(12) Forster, J.; Harriss-Phillips, W.; Douglass, M.; Bezak, E. A Review of the Development of Tumor Vasculature and Its Effects on the Tumor Microenvironment. *Hypoxia* **2017**, *5*, 21−32.
(13) Siemann, D. W. The Unique Characteristics of Tumor Vasculature and Preclinical Evidence for Its Selective Disruption by Tumor-Vascular Disrupting Agents. *Cancer Treat. Rev.* **2011**, *37* (1), 63−74.
(14) Bernabeu, M. O.; Köry, J.; Grogan, J. A.; Markelc, B.; Beardo, A.; d'Avezac, M.; Enjalbert, R.; Kaeppler, J.; Daly, N.; Hetherington, J.; Krüger, T.; Maini, P. K.; Pitt-Francis, J. M.; Muschel, R. J.; Alarcón, T.; Byrne, H. M. Abnormal Morphology Biases Hematocrit Distribution in Tumor Vasculature and Contributes to Heterogeneity in Tissue Oxygenation. *Proc. Natl. Acad. Sci. U. S. A.* **2020**, *117* (45), 27811−27819.
(15) Forster, J.; Harriss-Phillips, W.; Douglass, M.; Bezak, E. A Review of the Development of Tumor Vasculature and Its Effects on the Tumor Microenvironment. *Hypoxia* **2017**, *5*, 21−32.
(16) Charoenphol, P.; Huang, R. B.; Eniola-Adefeso, O. Potential Role of Size and Hemodynamics in the Efficacy of Vascular-Targeted Spherical Drug Carriers. *Biomaterials* **2010**, *31* (6), 1392−1402.
(17) Boyle, J. Microcirculatory Hematocrit and Blood Flow. *J. Theor. Biol.* **1988**, *131* (2), 223.
(18) Fitzgibbon, S.; Spann, A. P.; Qi, Q. M.; Shaqfeh, E. S. G. In Vitro Measurement of Particle Margination in the Microchannel Flow: Effect of Varying Hematocrit. *Biophys. J.* **2015**, *108* (10), 2601−2608.
(19) Hospital, H. G.; Medical, A. Vascular Wall Shear Stress: Basic Principles and Methods. *Hellenic J. Cardiol* **2005**, *46*, 9−15.
(20) Pries, A. R.; Secomb, T. W.; Gaehtgens, P. Structure and Hemodynamics of Microvascular Networks: Heterogeneity and Correlations. *Am. J. Physiol. Heart Circ. Physiol.* **1995**, *269*, 1713−1722.
(21) Reneman, R. S.; Hoeks, A. P. G. Wall Shear Stress as Measured in Vivo: Consequences for the Design of the Arterial System. *Med. Biol. Eng. Comput.* **2008**, *46* (5), 499−507.
(22) Namdee, K.; Thompson, A. J.; Charoenphol, P.; Eniola-Adefeso, O. Margination Propensity of Vascular-Targeted Spheres from Blood Flow in a Microfluidic Model of Human Microvessels. *Langmuir* **2013**, *29* (8), 2530−2535.
(23) Forouzandehmehr, M.; Shamloo, A. Margination and Adhesion of Micro- and Nanoparticles in the Coronary Circulation: A Step towards Optimised Drug Carrier Design. *Biomech. Model Mechanobiol.* **2018**, *17* (1), 205−221.
(24) Anselmo, A. C.; Modery-Pawlowski, C. L.; Menegatti, S.; Kumar, S.; Vogus, D. R.; Tian, L. L.; Chen, M.; Squires, T. M.; Sen Gupta, A.; Mitragotri, S. Platelet-like Nanoparticles: Mimicking Shape, Flexibility, and Surface Biology of Platelets to Target Vascular Injuries. *ACS Nano* **2014**, *8* (11), 11243−11253.
(25) Patil, V. R. S.; Campbell, C. J.; Yun, Y. H.; Slack, S. M.; Goetz, D. J. Particle Diameter Influences Adhesion under Flow. *Biophys. J.* **2001**, *80* (4), 1733−1743.
(26) Stroobach, M.; Haya, L.; Fenech, M. Effects of Red Blood Cell Aggregation on Microparticle Wall Adhesion in Circular Microchannels. *Med. Eng. Phys.* **2019**, *69*, 100−108.
(27) Doshi, N.; Prabhakarpandian, B.; Rea-Ramsey, A.; Pant, K.; Sundaram, S.; Mitragotri, S. Flow and Adhesion of Drug Carriers in Blood Vessels Depend on Their Shape: A Study Using Model Synthetic Microvascular Networks. *J. Controlled Release* **2010**, *146* (2), 196−200.
(28) Toy, R.; Hayden, E.; Shoup, C.; Baskaran, H.; Karathanasis, E. The Effects of Particle Size, Density and Shape on Margination of Nanoparticles in Microcirculation. *Nanotechnology* **2011**, *22* (11), 115101.
(29) D'Apolito, R.; Tomaiuolo, G.; Taraballi, F.; Minardi, S.; Kirui, D.; Liu, X.; Cevenini, A.; Palomba, R.; Ferrari, M.; Salvatore, F.; Tasciotti, E.; Guido, S. Red Blood Cells Affect the Margination of Microparticles in Synthetic Microcapillaries and Intravital Microcirculation as a Function of Their Size and Shape. *J. Controlled Release* **2015**, *217*, 263−272.
(30) Carboni, E. J.; Bognet, B. H.; Bouchillon, G. M.; Kadilak, A. L.; Shor, L. M.; Ward, M. D.; Ma, A. W. K. Direct Tracking of Particles and Quantification of Margination in Blood Flow. *Biophys. J.* **2016**, *111* (7), 1487−1495.
(31) MacFarlane, L.; Zhao, C.; Cai, J.; Qiu, H.; Manners, I. Emerging Applications for Living Crystallization-Driven Self-Assembly. *Chem. Sci.* **2021**, *12* (13), 4661−4682.
(32) Ganda, S.; Stenzel, M. H. Concepts, fabrication methods and applications of living crystallization-driven self-assembly of block copolymers. *Prog. Polym. Sci.* **2020**, *101*, 101195.
(33) Huo, H.; Zou, J.; Yang, S.; Zhang, J.; Liu, J.; Liu, Y.; Hao, Y.; Chen, H.; Li, H.; Huang, C.; Ungar, G.; Liu, F.; Zhang, Z.; Zhang, Q. Multicompartment Nanoparticles by Crystallization-Driven Self-Assembly of Star Polymers: Combining High Stability and Loading Capacity. *Macromol. Rapid Commun.* **2022**, *2200706*, 2200706.
(34) Ganda, S.; Wong, C. K.; Stenzel, M. H. Corona-Loading Strategies for Crystalline Particles Made by Living Crystallization-Driven Self-Assembly. *Macromolecules* **2021**, *54* (14), 6662−6669.
(35) Inam, M.; Jones, J. R.; Pérez-Madrigal, M. M.; Arno, M. C.; Dove, A. P.; O'Reilly, R. K. Controlling the Size of Two-Dimensional Polymer Platelets for Water-in-Water Emulsifiers. *ACS Cent Sci.* **2018**, *4* (1), 63−70.
(36) Inam, M.; Cambridge, G.; Pitto-Barry, A.; Laker, Z. P. L.; Wilson, N. R.; Mathers, R. T.; Dove, A. P.; O'Reilly, R. K. 1D: Vs. 2D Shape Selectivity in the Crystallization-Driven Self-Assembly of Polylactide Block Copolymers. *Chem. Sci.* **2017**, *8* (6), 4223−4230.
(37) Behnke, T.; Würth, C.; Hoffmann, K.; Hübner, M.; Panne, U.; Resch-Genger, U. Encapsulation of Hydrophobic Dyes in Polystyrene Microand Nanoparticles via Swelling Procedures. *J. Fluoresc.* **2011**, *21* (3), 937−944.
(38) Windberger, U.; Pöschl, C.; Peters, S.; Huber, J.; Van Den Hoven, R. Measurement of whole blood of different mammalian species in the oscillating shear field: Influence of erythrocyte aggregation. *J. Phys. Conf. Ser.* **2017**, *790* (1), 12035.
(39) Carboni, E. J.; Bognet, B. H.; Cowles, D. B.; Ma, A. W. K. The Margination of Particles in Areas of Constricted Blood Flow. *Biophys. J.* **2018**, *114* (9), 2221−2230.
(40) Qi, Q. M.; Shaqfeh, E. S. G. Time-Dependent Particle Migration and Margination in the Pressure-Driven Channel Flow of Blood. *Phys. Rev. Fluids.* **2018**, *3* (3), 1−18.
(41) Cooley, M.; Sarode, A.; Hoore, M.; Fedosov, D. A.; Mitragotri, S.; Sen Gupta, A. Influence of particle size and shape on their margination and wall-adhesion: implications in drug delivery vehicle design across nano-to-micro scale. *Nanoscale.* **2018**, *10* (32), 15350−15364.
(42) Müller, K.; Fedosov, D. A.; Gompper, G. Margination of micro- and nano-particles in blood flow and its effect on drug delivery. *Sci. Rep.* **2014**, *4*, 1−8.
(43) Wiedeman, M. P. Dimensions of Blood Vessels from Distributing Artery to Collecting Vein. *Circ. Res.* **1963**, *12*, 375.
(44) Semwogerere, D.; Weeks, E. R. Shear-Induced Particle Migration in Binary Colloidal Suspensions. *Phys. of Fluids* **2008**, *20* (4), 043306.
(45) Trebbin, M.; Steinhauser, D.; Perlich, J.; Buffet, A.; Roth, S. v.; Zimmermann, W.; Thiele, J.; Forster, S. Anisotropic Particles Align Perpendicular to the Flow Direction in Narrow Microchannels. *Proc. Natl. Acad. Sci. U. S. A.* **2013**, *110* (17), 6706−6711.
(46) Willcock, H.; O'Reilly, R. K. End Group Removal and Modification of RAFT Polymers. *Polym. Chem.* **2010**, *1* (2), 149−157.
(47) Evans, H. M.; Dootz, R.; Köster, S.; Struth, B.; Pfohl, T. X-Ray Microdiffraction on Flow-Controlled Biomolecular Assemblies. *Bull. Polish Acad. Sci. Technol. Sci.* **2007**, *55* (2), 217−227.

https://doi.org/10.1021/acsmacrolett.2c00718
ACS Macro Lett. 2023, 12, 344−349